Isothermal Crystallization Kinetics and Melting Behavior of Multiwalled Carbon Nanotubes/Polyamide-6 Composites

Juan Li,[1] Zhengping Fang,[1] Yan Zhu,[1] Lifang Tong,[1] Aijuan Gu,[1] Fu Liu[2]

[1]*Institute of Polymer Composites, Zhejiang University, Hangzhou 310027, Zhejiang, China*
[2]*Institute of Material Physics and Microstructure, Zhejiang University, Hangzhou 310027, Zhejiang, China*

Received 11 November 2005; accepted 13 March 2006
DOI 10.1002/app.24606
Published online 5 June 2007 in Wiley InterScience (www.interscience.wiley.com).

ABSTRACT: Pristine and functionalized multiwalled carbon nanotubes (MWNTs) were used to fabricate polyamide 6 (PA6) composites through melt blending. The functionalized MWNTs were obtained by grafting 1,6-hexamethylenediamine (HMD) onto the pristine MWNTs to improve their compatibility with PA6 matrix. The effect of MWNTs on the isothermal crystallization and melting behavior of PA6 was investigated by differential scanning calorimetry (DSC) and X-ray diffraction (XRD). The Avrami and Lauritzen–Hoffmann equations are used to describe the isothermal crystallization kinetics. The values of the Avrami exponent found for neat PA6, the pristine MWNTs/PA6 and functionalized MWNTs/PA6 composite samples are about 4.0, 1.7, and 2.3, respectively. The activation energies are determined by the Arrhenius method, which is lower for the composites, −320.52 KJ/mol for pristine MWNTs/PA6 and −293.83 KJ/mol for functionalized MWNTs/PA6, than that for the neat PA6 (−284.71 KJ/mol). The following melting behavior reveals that all the isothermally crystallized samples exhibit triple melting endotherms at lower crystallization temperature and double melting endotherms at higher crystallization temperature. The multiple melting endotherms are mainly caused by the recrystallization of PA6 during heating. The resulting equilibrium melting temperature is lower for the composites than for neat PA6. In addition, polarizing microscopy (PLM) and small angle light scanning (SALS) were used to study the spherulite morphology. The results show that the MWNTs reduce the spherulite radius of PA6. This reduction is more significant for pristine MWNTs. © 2007 Wiley Periodicals, Inc. J Appl Polym Sci 105: 3531–3542, 2007

Key words: polyamides; multiwalled carbon nanotubes; amino-functionalization; composites; crystallization

INTRODUCTION

Polyamide 6 (PA6) is a typical thermoplastic that has a wide range of engineering applications. In practice, introducing fillers in PA6 is an effective and common method to improve the properties of PA6. While carbon nanotube (CNT), which has remarkable physical and mechanical properties, is considered as an ideal reinforcing material for polymer composites, the fabrication and properties of CNTs/PA6 composites have gained much attention.[1–3] The challenges for developing high-performance CNTs/polymer composites are: uniform dispersion of CNTs in polymer matrix, and strong interfacial adhesion between CNTs and the matrix.[4–6] To address the two questions, many methods have been adopted to modify the surface characteristics of CNTs. Among all, grafting functional groups onto CNTs is one of the most feasible ways according to recent publications.[7–14] Based on the structure of PA6, 1,6-hexamethylenediamine (HMD) was used to modify the surface of multiwalled carbon nanotubes (MWNTs), which has been reported in our previous work. A better compatibility between amino-functionalized MWNTs (f-MWNTs) and PA6, and a more uniform dispersion of f-MWNTs in PA6 has been achieved.[15,16]

The structure of CNTs/polymer composites is another focus of interest. For PA6, which is a semicrystalline polymer, its physical, chemical, and mechanical properties depend greatly on the crystalline structure, the degree of crystallization, and the crystalline morphology. The crystalline structures observed in PA6 mainly fall in two categories: α and γ.[17–19] The α phase is composed of a fully extended planar zigzag chain conformation, in which adjacent antiparallel chains are joined to each other by hydrogen bonds. Therefore, it is the most thermodynamically stable crystalline form, and can be obtained by slowly cooling from the melt. The pseudohexagonal γ phase consists of pleated sheets of parallel chains joined by hydrogen bonds. It is less stable and can be obtained by fast cooling from the melt or fiber spinning at a high speed.[20,21] The γ form can be converted into α by recrystallization, by applying stress at room temperature, and by thermal annealing in a

Correspondence to: Z.-p. Fang (zpfang@zju.edu.cn).

saturated-steam atmosphere without any significant loss of orientation.[22–25]

Besides the factors mentioned above, the type and surface characteristics of fillers have an important effect on the crystallization behavior of PA6. To control the crystallization rate and the degree of crystallinity and to obtain the desired morphology and properties, great efforts have been devoted into studying the effect of some fillers, such as ZnO, montmorillonite, and foliated graphite,[26–28] on the crystallization behavior of PA6. There have been also a few papers dealing with the crystallization behavior of CNTs/polymer composites.[29–31] Recently, Liu et al.[32] mentioned the effect of annealing on the crystallization and melting behavior of MWNTs/PA6 composites, while there have been few paper focusing on the crystallization kinetics of MWNTs/PA6 composites.

In this study, MWNTs/PA6 composites were prepared via melt blending. The influence of pristine MWNTs (p-MWNTs) and f-MWNTs on the isothermal crystallization kinetics and melting behavior of PA6 was investigated using differential scanning calorimetry (DSC) and X-ray diffraction (XRD). The kinetics data were analyzed using the Avrami and Lauritzen–Hoffmann equation, and the activation energies for isothermal crystallization were evaluated. The crystalline structure and morphology were also obtained with polarizing microscopy (PLM) and small angle light scanning (SALS).

EXPERIMENTAL

Materials

PA6 pellets (CM1017) used in this study were obtained commercially from Toray Japan with a number average molecular weight 25,000 g/mol. MWNTs were provided by Institute of Material Physics and Microstructure at Zhejiang University (China), which was prepared by the catalytic decomposition of acetylene at 700 °C for ~60 min. The p-MWNTs were purified by soaking in nitric acid for 48 h at room temperature to remove the catalyst article and impurities. The f-MWNTs were obtained by grafting HMD onto the p-MWNTs via chemical methods. Detailed procedures for the preparation of f-MWNTs have been described in our previous paper.[15]

Preparation of MWNTs/PA6 composites

The MWNTs/PA6 composites were prepared via a melt-blending method using a PRISM TSE-16-TC Brabender twin-screw extruder. The temperature of the extruder was maintained at 185, 228, 238, 238, and 225°C from hopper to die respectively. The rotation speed of the twin screw was 30 rpm. The composites containing 1.0 wt % MWNTs was studied in this paper. Neat PA6 was also extruded at the same condition. All the samples were dried under vacuum at 80°C for 24 h to remove any residual water before testing.

Differential scanning calorimetry

Perkin–Elmer Pyris 1 DSC thermal analyzer was used to analyze the isothermal crystallization and subsequent melting behavior. The instrument was calibrated with high purity indium and zinc standards. About 4–6 mg of the polymer samples were weighed accurately in the aluminum pans. All DSC analyses were performed under nitrogen atmosphere. The isothermal crystallization and melting process of PA6 were performed as follows: the samples were heated at 40°C/min to 245°C and melt there for 4 min to erase all previous thermal history. Then they were cooled at 100°C/min to the predetermined crystallization temperature, T_c, in the range 188–200 °C in steps of 2°C, and maintained at T_c for 20 min necessary for the crystallization process completed. Additionally, the crystalline samples were quickly cooled to 50°C, maintained at this temperature for 4 min, and heated to 250°C at a rate of 10°C/min. Both the exothermic and endothermic curves were recorded.

X-ray diffraction

XRD patterns were recorded using a Rigaku D/Max-2550 diffractometer. The CuKa radiation (λ = 0.15418 nm) source was operated at 40 kV and 300 mA. Patterns were recorded by monitoring those diffractions that appeared from 5° to 45°. The scan speed was 10°/min. The film samples were melted at 250°C for 10 min and then transferred to an oven with preset crystallization temperature (190°C) for 2 h.

Polarizing microscopy

PLM observations were made with a XP-203 polarizing microscope (Changfang Optical Instrument, Shanghai, China) equipped with a hot stage and CCD camera. Samples were melted at 250°C between two glass slides to obtain thin films and maintained at this temperature for 10 min. The films were transferred onto another hot stage with preset crystallization temperature (T_c = 200°C) for 12 h.

Small angle light scattering

A 2 mW 632.8 nm He–Ne with beam size 1 mm was used as the source of SALS. The samples were the

same as that for PLM. The H_v diffraction patterns of SALS were obtained by applying the Bertran lens. The average dimensions of the spherulites were determined from the H_v patterns, using the Stein equation.[33]

RESULTS AND DISCUSSION

Isothermal crystallization kinetics analysis

Isothermal crystallization kinetics analysis based on the Avrami equation

Figure 1 shows the isothermal crystallization exotherms of neat PA6 and MWNTs/PA6 composites with MWNTs content of 1.0 wt %. It is seen that for all the samples, the crystallization exothermic peak becomes flatter, and the time to reach the maximum degree of crystallization increases, as the crystallization temperature increases. From Figure 1(b,c), one can also read that at all the crystallization temperatures adopted similar pattern, a significant portion of PA6 crystallizes before timing begins. This implies that the temperature at which the crystallization of the PA6 in the composite starts is higher than that of the neat one.

The Avrami equation[34,35] is applied to analyze the isothermal crystallization of PA6 and its composites, as given in eq. (1):

$$X(t) = 1 - \exp(-Kt^n) \tag{1}$$

where K is the Avrami rate constant containing the nucleation and the growth parameters, n is the Avrami exponent whose value depends on the mechanism of nucleation and on the form of crystal growth, t denotes the real time of crystallization (the elapsed time deducting crystallization induction time). $X(t)$ is related to the relative crystallinity at time t. $X(t)$ can be obtained from the ratio of the area of the exotherm up to time t divided by the total exotherm as follows:

$$X(t) = \frac{\int_0^t (dH/dt)dt}{\int_0^\infty (dH/dt)dt} \tag{2}$$

where dH denotes the measured enthalpy of crystallization during an infinitesimal time interval dt, ∞ is the time at the end of the crystallization process. Figure 2 presents the $X(t)$ as a function of t for PA6, p-MWNTs/PA6, and f-MWNTs/PA6 composites. As can be seen, all the isotherms exhibit a sigmoid dependence with time. The characteristic isotherms are shifted to right along the time axis with increase of crystallization temperature, indicating progressively slower crystallization rate. A slow increase of crystallinity with time after most of the crystallization had taken place is observed and this is attributed to the presence to secondary crystallization.[33] From these curves, the half-time of crystallization, $t_{1/2}$, can be directly determined as the time elapsed from the onset of crystallization to the point where the crystallization is half completed. The $t_{1/2}$ values and the

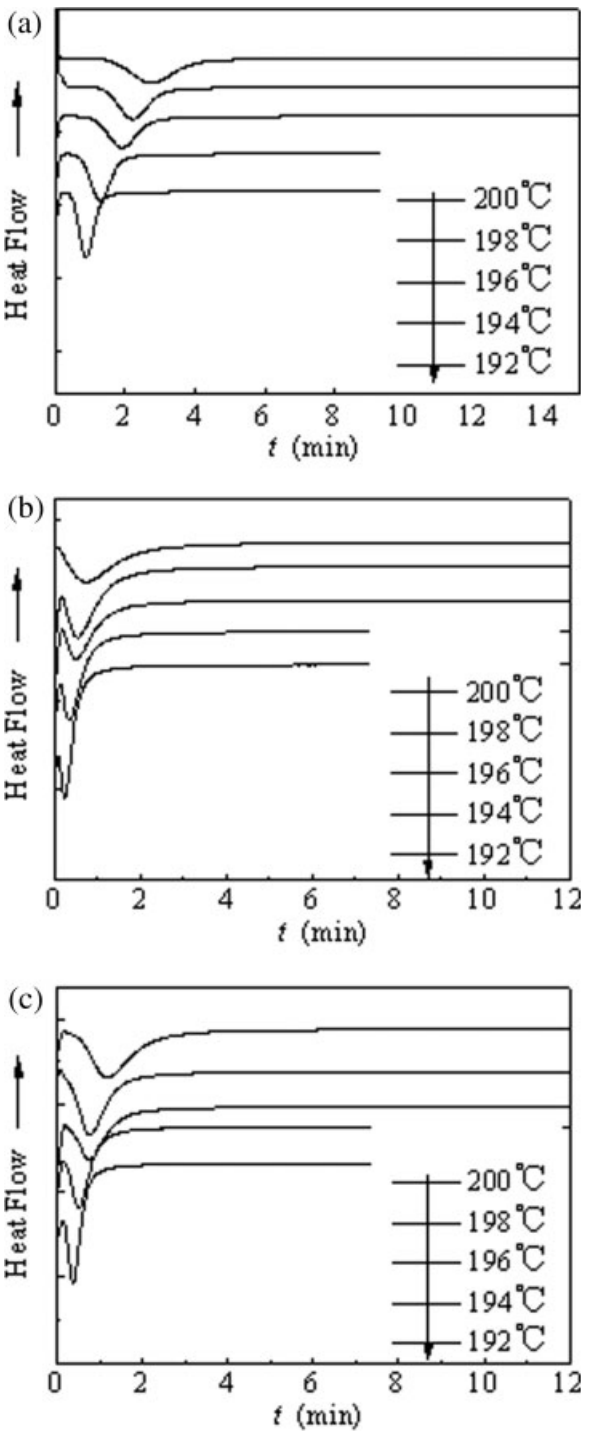

Figure 1 Heat flow as a function of time during isothermal crystallization at the different crystallization temperatures by DSC for (a) PA6 (b) p-MWNTs/PA6 and (c) f-MWNTs/PA6 composites with 1.0 wt % MWNTs.

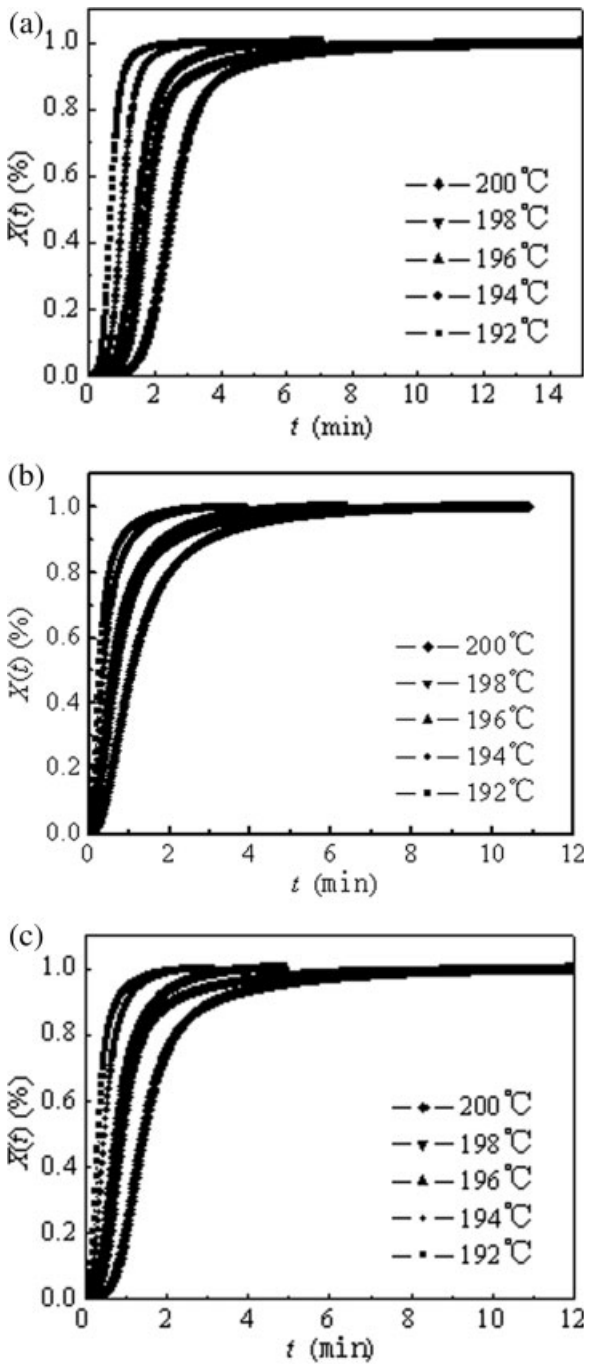

Figure 2 Relative crystallinity versus crystallization time for various crystallization temperatures from DSC thermograms of (a) PA6 (b) p-MWNTs/PA6 and (c) f-MWNTs/PA6 composites with 1.0 wt % MWNTs.

crystallization parameters, ΔH, are summarized in Table I.

Take its double logarithmic form, eq. (1) can be rearranged as

$$\ln[-\ln(1 - X(t))] = \ln K + n \ln t \quad (3)$$

From this expression one can expect that if the Avrami approach is valid the plot of $\ln[-\ln(1 - X(t))]$ versus $\ln t$ should be a straight line for which the slope is equal to n and the intercept is $\ln K$. Figure 3 shows the plots of $\ln[-\ln(1 - X(t))]$ versus $\ln t$ for the neat PA6 and p-MWNTs/PA6 and f-MWNTs/PA6 composites. It is seen that straight lines are obtained for all the samples with a relative crystallinity ranged from 0.5 to 80%. Beyond 80%, the curves deviate from the linear stage, which is attributed to the secondary crystallization. Many results have suggested that both primary and secondary crystallization were incorporated into Avrami theory. In the present work, we focus on the primary crystallization. For comparison, the region of about 1–75% conversion in the curves for all the sample is chosen to determine the exponent n and K according to eq. (3) and the results are presented in Table I.

The n values of the neat PA6 vary from 3.8 to 4.4, and those of the p-MWNTs/PA6 and f-MWNTs/PA6 composites range around 1.5–1.7 and 2.1–2.5,

TABLE I
Parameters of the Isothermal Crystallization for Neat PA6 and its Composites

	T_c (°C)				
	192	194	196	198	200
PA6					
n	3.78	4.01	3.81	4.35	4.36
K^a	2.70	0.55	0.14	0.05	0.01
K^b	2.76	0.55	0.14	0.06	0.01
$t_{1/2}$ (min)^a	0.69	1.06	1.51	1.79	2.53
$t_{1/2}$ (min)^b	0.70	1.06	1.51	1.82	2.57
$\tau_{1/2}$ (min^{-1})^a	1.44	0.94	0.66	0.56	0.39
$\tau_{1/2}$ (min^{-1})^b	1.43	0.94	0.66	0.55	0.39
t_{max} (min)^c	0.73	1.00	1.45	1.74	2.45
t_{max} (min)^d	0.71	1.08	1.53	1.86	2.63
ΔH (J/g)	53.62	52.61	51.24	68.81	69.77
p-MWNTs/PA6					
n	1.72	1.67	1.53	1.62	1.73
K^a	7.18	3.25	1.53	1.19	0.59
K^b	6.75	3.42	1.65	1.25	0.66
$t_{1/2}$ (min)^a	0.27	0.39	0.57	0.69	1.06
$t_{1/2}$ (min)^b	0.26	0.40	0.60	0.72	1.10
$\tau_{1/2}$ (min^{-1})^a	3.76	2.60	1.76	1.44	0.95
$\tau_{1/2}$ (min^{-1})^b	3.89	2.52	1.68	1.39	0.91
t_{max} (min)^c	0.17	0.22	0.32	0.38	0.68
t_{max} (min)^d	0.19	0.29	0.38	0.49	0.82
ΔH (J/g)	16.02	18.49	19.46	32.86	49.54
f-MWNTs/PA6					
n	2.14	2.19	2.18	2.36	2.47
K^a	6.60	3.12	1.20	0.94	0.33
K^b	6.87	3.25	1.26	1.02	0.35
$t_{1/2}$ (min)^a	0.34	0.49	0.76	0.85	1.32
$t_{1/2}$ (min)^b	0.35	0.50	0.78	0.88	1.35
$\tau_{1/2}$ (min^{-1})^a	2.92	2.03	1.32	1.18	0.76
$\tau_{1/2}$ (min^{-1})^b	2.87	1.99	1.29	1.14	0.74
t_{max} (min)^c	0.25	0.37	0.58	0.70	1.05
t_{max} (min)^d	0.31	0.45	0.69	0.81	1.27
ΔH (J/g)	25.10	26.96	29.24	66.22	68.37

[a] Determined from Figure 2.
[b] Determined from eq. 4.
[c] Determined from figure 1.
[d] Determined from eq. 8.

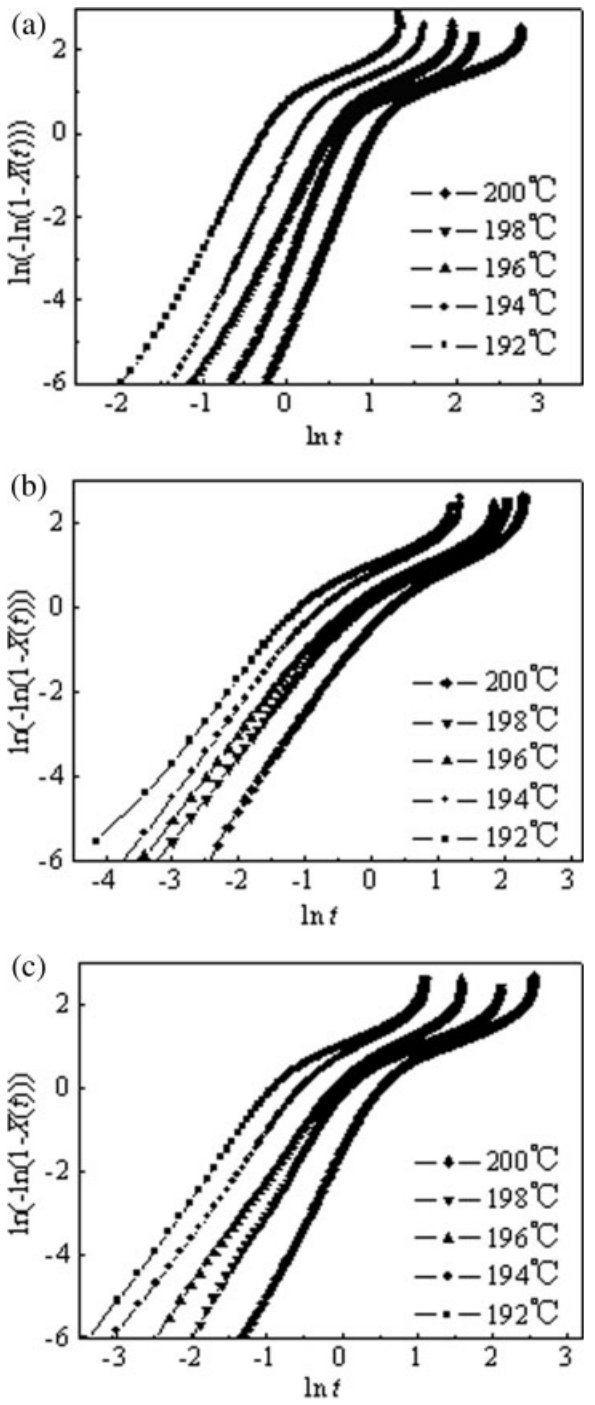

Figure 3 Plots of $\ln[-\ln(1-X(t))]$ versus $\ln t$ for (a) PA6 (b) p-MWNTs/PA6 and (c) f-MWNTs/PA6 composites with 1.0 wt % MWNTs isothermally crystallized at indicated temperature.

respectively. The values of exponent n for neat PA6 are close to 4.0, which mean that PA6 chains tend to take the 3D growth mechanism. With the addition of the MWNTs, the mechanism of nucleation and the growth of PA6 crystallite are greatly influenced, leading to the decrease of the Avrami exponent n in the composites. The growth of crystals in p-MWNTs/PA6 composite melt is probably 2D, and the nucleation process is heterogeneous and simultaneous under the experimental conditions. After grafting HMD, the compatibility between PA6 and MWNTs is increased, thus promotes the PA6 chains in f-MWNTs/PA6 composite taking a growth mechanism of the combination of 2D and 3D.[36]

The half-time of crystallization, $t_{1/2}$, is an important parameters for the analysis of crystallization kinetics, which is defined as the time at which the extent of crystallization is 50%. It can be conveniently extracted from the plots of relative crystallinity $X(t)$ versus time t in Figure 2 as mentioned above. With $X(t) = 0.5$, from eq. (3) the relation between the half-time and the crystallization parameter K can be expressed as

$$t_{1/2} = (\ln 2/K)^{1/n} \tag{4}$$

with n the Avrami exponent. Using eq. (4), the theoretical values of K and $t_{1/2}$ can be calculated if take one of them from the experimental data. The values of the half-time $t_{1/2}$ and the crystallization parameter K derived both from experimental data and eq. (4) are listed in Table I. As can be seen, the values of $t_{1/2}$ and K derived from eq. (4) agree well with those obtained from the experimental plots.

From the data in Table I, it is apparent that the values of $t_{1/2}$ for both composites are lower than the for neat PA6. Usually, $t_{1/2}$ or the reciprocal of $t_{1/2}$, $\tau_{1/2}$, is directly used to describe the rate of crystallization. The greater the value of $t_{1/2}$, the lower is the rate of the crystallization. The reciprocal of $t_{1/2}$, as a function of the crystallization temperature, T_c, is presented in Figure 4 for the neat PA6 and its composites. It can be seen that at all temperatures the rate of crystallization of PA6 is always lower than the corresponding values of the composites. This is due to the nucleating effect of MWNTs. Further-

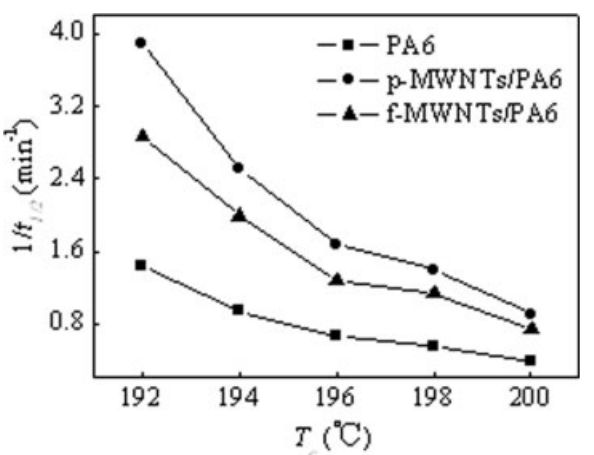

Figure 4 Plots of the reciprocal half crystallization time versus crystallization temperature for PA6 and its composites.

more, the p-MWNTs/PA6 have a higher rate of crystallization than have the f-MWNTs/PA6 at the same temperatures, which indicate increased interaction between f-MWNTs and PA6 limiting the diffusion of PA6 chains. This hindrance is more obvious at higher temperature, and so the increase of the rate of crystallization is lesser than that at lower temperature. In addition, for all the samples the $t_{1/2}$ increases with T_c, in agreement with the kinetics theory of crystallization, which expects for crystallization close to the melting temperature, a decrease of undercooling will induce a reduction in $1/t_{1/2}$.

Spherulite growth analysis

It has been suggested that the kinetic data of isothermal crystallization can be analyzed with the growth rate of the spherulites in the context of Lauritzen–Hoffman secondary nucleation theory.[37] According, the temperature dependence of the linear growth rate (G) is given as follows:

$$G = G_0 \exp\left(-\frac{U^*}{R(T_c - T_\infty)}\right) \exp\left(-\frac{K_g}{T_c(\Delta T)f}\right) \quad (5)$$

where G_0 is a preexponential factor, U^* is the energy for the transport of the macromolecules in the melt and is commonly given by a universal value of 6280 J/mol, T_∞ is a hypothetical temperature below which all the motions associated with the viscous flow ceases, defined as $T_g - C$ where T_g is the glass transition temperature and C is a constant equal to 30, R is the universal gas constant, ΔT is the undercooling defined as $T_m^0 - T_c$, T_m^0 is the equilibrium melting temperature, f is a corrective factor for the decrease of the enthalpy of fusion with the crystallization temperature, $f = 2T_c/(T_c + T_m^0)$. K_g is a nucleation parameter related to the fold and lateral surface energies. For a secondary or heterogeneous nucleation, K_g can be calculated from:

$$K_g = \frac{n\sigma\sigma_e b_0 T_m^0}{\Delta h_f \rho_c k_B} \quad (6)$$

where n takes the value of 4 when crystallization takes place in regime I or III and the value of 2 in regime II, σ and σ_e are the side surface (lateral) and fold surface free energies that measure the work required to create a new surface, b_0 is the single layer thickness, $\Delta h_f \rho_c = \Delta H_f$ is the enthalpy of melting per unite volume, and k_B is the Boltzmann constant. The nucleation parameters, K_g, can be calculated from eq. (5) with the double logarithmic transformation:

$$\ln G + \frac{U^*}{R(T_c - T_\infty)} = \ln G_0 - \frac{K_g}{T_c(\Delta T)f} \quad (7)$$

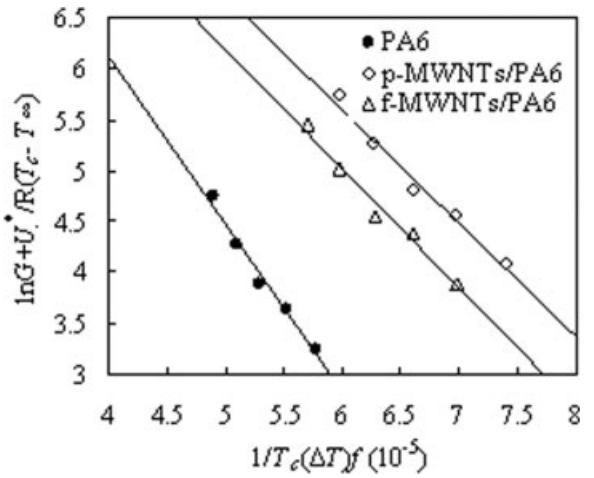

Figure 5 Plots of $\ln G + U^*/R(T_c - T_\infty)$ versus $1/T_c(\Delta T)f$ for the neat PA6 and its composites

It is generally accepted that these crystallization rate parameters are related in some way to the primary nucleation rate and to the subsequent crystal growth rate. With $1/t_{1/2}$ or $\tau_{1/2}$ instead of G, drawing a straight line of the left-hand side of eq. (7) against $1/T_c(\Delta T)f$ will give a slope of $-K_g$. Using the obtained values of T_m^0 in the following case and T_g = 323 K for PA6, the relationship between $\ln G + U^*/R(T_c - T_\infty)$ and $1/T_c(\Delta T)f$ is represented in Figure 5, and the values of the nucleation parameter K_g are derived from the slopes as 1.63×10^5, 1.14×10^5, and 1.17×10^5 K^2 for neat PA6, p-MWNTs/PA6, and f-MWNTs/PA6 composites, respectively. It is clear that the addition of MWNTs decreases the value of K_g, and this decrease is more obvious for p-MWNTs/PA6. It is well known that a foreign surface reduces frequently the nucleus size for crystal growth since the creation of the interface between polymer crystal and substrate may be less hindered than the creation of the corresponding free polymer crystal surface.[38] A heterogeneous nucleation path makes use of a foreign preexisting surface to reduce the free energy opposing primary nucleation. It is thus verified that the existence of the MWNTs reduces the work needed to create a new surface leading to faster crystallization.

Additionally, the time to reach the maximum rate of crystallization t_{max} can also be used to characterize the rate of crystallization. The data of t_{max} can be easily found from the isotherms in Figure 1, and the values at various crystallization temperature are all tabulated in Table I. Since t_{max} corresponds to the point at which $dQ(t)/dt = 0$, $Q(t)$ is the rate of heat evolution, thus

$$t_{max} = [(n-1)/nK]^{1/n} \quad (8)$$

the value of t_{max} can be derived from the Avrami exponent n and the parameter K obtained from the

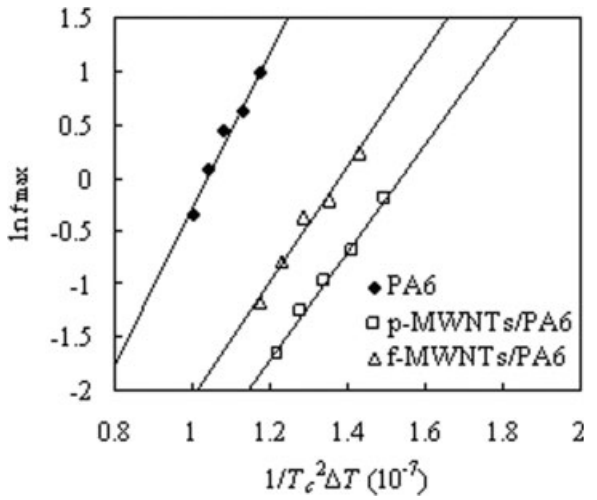

Figure 6 Plots of $\ln t_{max}$ versus $1/(T_c^2\Delta T)$ for the neat PA6 and the composites sample.

plots of $\ln[-\ln(1-X(t))]$ versus $\ln t$. Both the calculated and the extracted values of $t_{\max}$ are listed in Table I. It is clear that the values of most of the crystallization parameters calculated using the theoretical equations are in good agreement with those obtained from the experimental plots, suggesting that the Avrami analysis works very well in describing the crystallization of PA6 from the melt of neat PA6 and the composites.

To investigate the dependence of the spherulite growth rate upon the crystallization temperature, Lin[39] derived the following relation:

$$\ln t_{\max} = A - \frac{B}{T_c^2 \Delta T} \tag{9}$$

where A and B are constants, the other variables are the same as defined previously. Equation (9) can be used to verify the possibility that the PA6 and its composites could be described by Avrami equation at the primary stage of the isothermal crystallization. This means that if the plot of $\ln t_{\max}$ versus $1/T_c^2\Delta T$ is a straight line, then it is possible that PA6 macromolecules undergo primary crystallization at $t_{\max}$ in the neat PA6 and the composites samples. The plot is shown in Figure 6, and it has a linear relation.

Crystallization activation energy

The crystallization process for bulk PA6 is assumed to be thermally activated, thus the Avrami parameter K can be used to determine the energy for crystallization. The crystallization rate parameter K can be approximately described by the Arrhenius[40] equation such that

$$K^{1/n} = k_0 \exp(-\Delta E_a/RT_c)$$

or

$$1/n(\ln K) = \ln k_0 - \Delta E_a/RT_c \tag{10}$$

where k_0 is a temperature independent preexponential factor, ΔE is an activation energy, R is the gas constant, and T_c is the crystallization temperature. From a graphic representation (Fig. 7) of the experimental data of $1/n \ln K$ against $1/T_c$, ΔE can be determined by the slope of the linear plot. The values of the crystallization activation energy are found to be -284.71, -320.52 and -293.83 kJ/mol for the neat PA6 and the p-MWNTs/PA6 and f-MWNTs/PA6 composites, respectively. The results indicate that the addition of MWNTs into PA6 probably induces heterogeneous nucleation (a lower ΔE). Since transforming the molten fluid into the crystalline state involves the release of energy, a greater magnitude of ΔE ($|\Delta E|$) means that the transformation need to release more energy suggesting a more difficult motion of PA6 chains in the composites. Better compatibility between f-MWNTs and PA6 decrease heterogeneous nucleation ability of MWNTs, resulting in a higher ΔE (lower $|\Delta E|$) for f-MWNTs/PA6 than for p-MWNTs/PA6. It is well known that the crystallization process of PA6 involves two important steps, that is, the nucleation and the diffusion of crystallizable chains to the crystal front. Incorporating MWNTs in PA6 induces the heterogeneous nucleation of PA6 chains; therefore, the crystallization rates are increased. However, with the crystal growth, the stiff MWNTs or even the aggregation of these tubes may hinder the transportation of PA6 chains resulting in a higher $|\Delta E|$. The nucleation effect is superior over the hindrance of PA6 chains caused by the MWNTs. Therefore the composites have higher crystallization rate than have neat PA6.

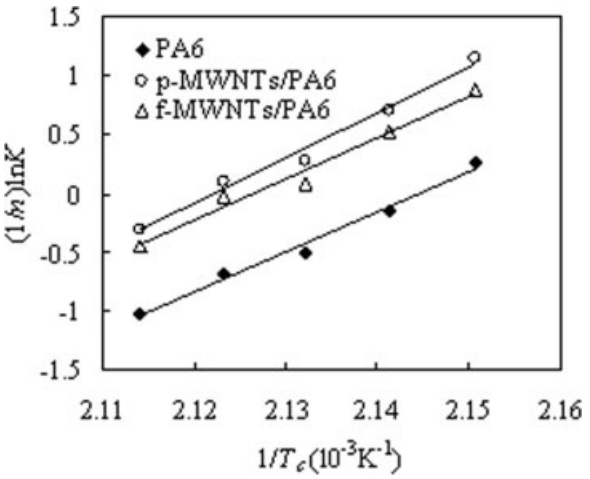

Figure 7 Plots of $1/n\ln K$ versus $1/T_c$ for the neat PA6 and the composites sample.

Melting behavior and equilibrium melting temperature

Figure 8 presents a series of DSC heating thermograms of neat PA6, p-MWNTs/PA6, and f-MWNTs/PA6 composites after crystallization at different crystallization temperature(T_c). The related data are listed in Table II. It is apparent that the DSC endotherms exhibit triple melting peaks at lower T_c and double melting peaks at higher T_c. The first and smallest endotherm (referred as T_m^{I}) is found to start at about 5°C above T_c in all samples. The peak position of T_m^{I} which is associated with the last step of secondary crystallization shifts to higher temperatures as T_c increase. The second and third endotherm (referred as T_m^{II} and T_m^{III}), associated with the fusion of crystals grown at T_c. The triple melting sequence reverts to double melting behavior at 200°C due to the combination of an increase of peak II with a decrease of peak III.[26]

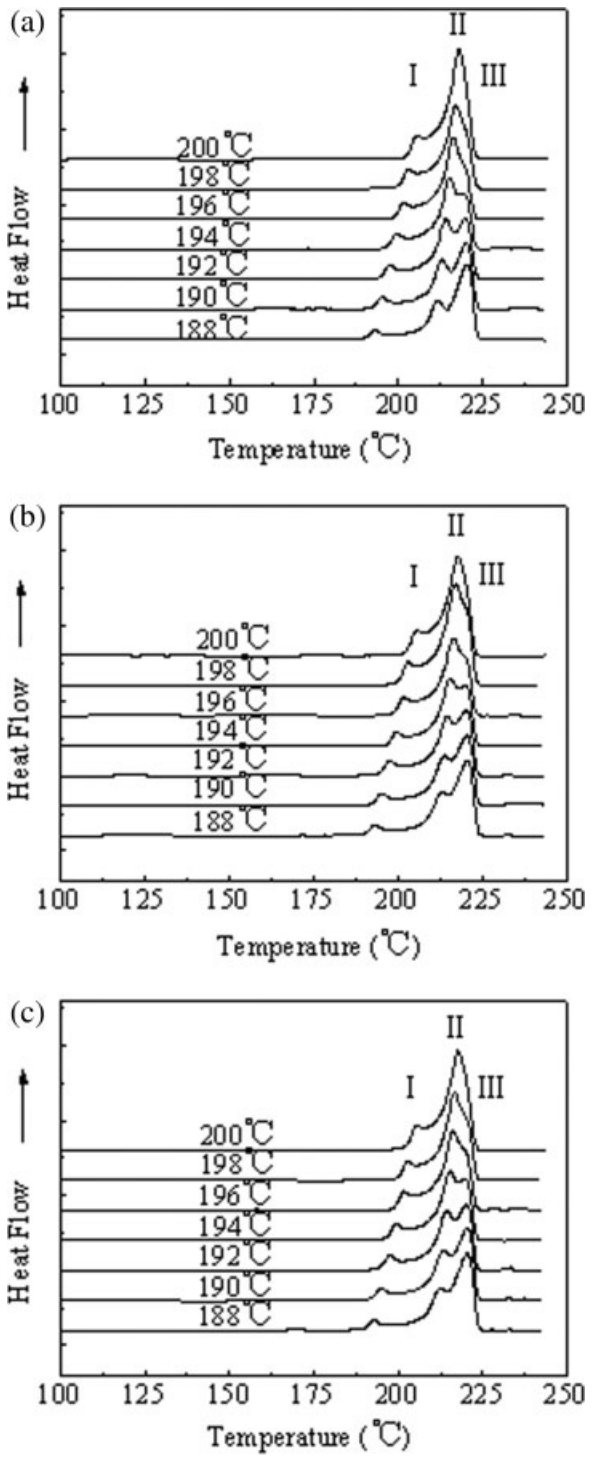

Figure 8 Melting endotherms of (a) PA6 (b) p-MWNTs/PA6 and (c) f-MWNTs/PA6 composites after isothermal crystallization at the specified temperature, recorded at the heating rate of 10 °C/min.

The double melting endotherms (peak II and III) formed in the primary crystallization process are probably caused by two different crystal structures, different crystal sizes, and perfection during heating.[41–43] Many researchers have detected the polymorphism behavior of PA6, which is dependent on the crystallization conditions strongly.[44–46] Medellín-Rodríguez[46] investigated the melting behavior of PA6 after isothermal crystallization from 80 to 200°C. They found that PA6 exhibit α form at high temperature (>160°C), and the α form shows the thermal sequence from triple to double melting behavior as the T_c increase(>180°C). In our present research, the crystallization temperatures of PA6 change from 188 to 200°C, and the melting behavior undergoes a transformation from triple to double melting peaks. It is considered that these melting peaks should correspond to the melting of α crystalline form for PA6 as supported by the following XRD results. Then the multiple thermograms may attribute to the spherulites with different size and perfection, which melt and recrystallize during DSC heating. At higher temperature, more perfect crystals are formed and they start to melt at higher temperature. The recrystallization effect is weakened, resulting in the single peak for the samples crystallized at 200°C.

Comparing the thermograms of the neat PA6 and the composites in Table II, it is found the peaks have almost the same form and transformation. However, the temperature of the main melting peak T_m^{II} for the composite samples are higher than that for the neat PA6 at lower temperature, such as 188°C, but are lower than that for the neat PA6 at a higher temperature 200°C, which suggests less perfection of the crystals in the composite samples at a high crystallization temperature. This further confirms that the presence of MWNTs hinder the transportation of the PA6 chains and thus decrease the spherulites size and perfection as shown in Figure 11. The higher the temperature, the better the mobility of PA6 is. Therefore, the hindrance of these stiff MWNTs is more obvious. This is consistent with the results observed in treating the isothermal crystallization

TABLE II
Values of Melting Point (T_m) and Melting Enthalpy (ΔH_f) of the PA6 and its Composites Melting at a Heating Rate of 10°C/min after Isothermal Crystallization at Indicated Temperature T_c

	T_c (°C)						
	188	190	192	194	196	198	200
PA6							
T_m^0	192.84	195.21	197.05	199.60	201.64	203.12	205.59
T_m^{II}	211.61	212.92	213.99	215.18	216.22	216.98	217.94
T_m^{III}	220.16	220.01	219.86	219.04	–	–	–
ΔH_f (J/g)	62.65	62.54	63.20	62.23	62.75	76.14	77.03
p-MWNTs/PA6							
T_m^I	193.28	195.33	197.73	199.78	201.85	203.221	205.55
T_m^{II}	213.07	213.77	214.49	215.54	216.42	217.08	217.73
T_m^{III}	220.45	220.32	220.03	219.73	–	–	–
ΔH_f (J/g)	68.57	66.57	65.82	66.22	65.24	86.66	76.12
f-MWNTs/PA6							
T_m^I	192.79	195.00	197.40	199.46	201.86	202.95	205.55
T_m^{II}	212.58	213.45	214.33	215.38	216.26	216.63	217.73
T_m^{III}	220.29	220.32	220.03	219.57	–	–	–
ΔH_f (J/g)	64.62	66.75	67.09	66.68	66.01	75.07	79.11

kinetics using Avrami theory. The increase of $1/t_{1/2}$ for composites is higher at lower crystallization temperature than at higher crystallization temperature.

Figue 9 shows the plot of T_m versus T_c. It is evident that T_m values exhibit a linear relationship with T_c. From both Figures 8 and 9(a), we can see that T_m^I varies linearly with T_c, but it is almost parallel with the line $T_m = T_c$. The T_m^{III} decreases as T_c increases. Thus the resulting the equilibrium melting temperature (T_m^0) would below the T_m^{III} which is unreasonable. Because both peak I and III are useless in the determination of the T_m^0 of PA6, peak II is selected to calculate the T_m^0. According to the theory derived by Hoffman and Weeks,[47] the T_m^0, which is the melting temperature of infinitely extended crystals, can be obtained by linear extrapolation of T_m^{II} versus T_c data to the line $T_m = T_c$. Mathematically, they arrived at the following equation:

$$T_m = \frac{T_c}{2\beta} + T_m^0\left[1 - \frac{1}{2\beta}\right] \quad (11)$$

where T_m^0 is the equilibrium melting point and β is the ''thickening ratio.'' In other words, β indicates the ratio of the thickness of the mature crystal L_c to that of the initial one L_c^*, therefore, $\beta = L_c/L_c^*$, which describes the growth of the lamellar thickness during crystallization and is supposed to be always be greater than or equal to 1. From Figure 9(b), we obtain the T_m^0 values of 510.92, 502.86, 504.27 K and β values of 0.95, 1.26 and 1.16 for neat PA6, p-MWNTs/PA6, and f-MWNTs/PA6 composites, respectively (listed in Table III). The addition of MWNTs decreases the value of T_m^0. The reason for

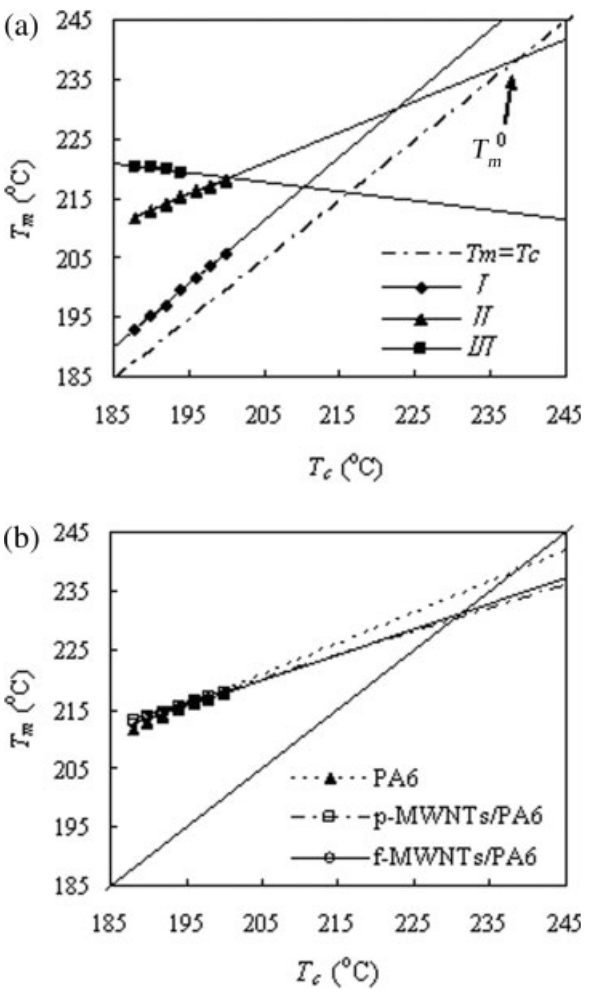

Figure 9 Melting temperature as a function of crystallization temperature for (a) PA6 and (b) PA6 and its composites.

TABLE III
Values of ΔE_a, T_m^0, β, K_g, G_0, at Various T_c for the PA6 and its Composites

Samples	ΔE_a (kJ/mol)	T_m^0 (K)	β	K_g (K^2)	G_0 (min^{-1})
PA6	−284.71	510.92	0.95	1.63 E +05	3.20 E +05
p-MWNTs/PA6	−320.52	502.86	1.26	1.14 E +05	2.37 E +05
f-MWNTs/PA6	−293.83	504.27	1.16	1.17 E +05	1.69 E +05

such changes could be reasonably interpreted by the different interaction between MWNTs and PA6, and in PA6 chains itself, which induces the formation of various crystalline structure in PA6.

Crystalline structure

Figure 10 shows XRD data of PA6 and its composites. For all the samples, the XRD results show only the presence of two intense reflections (100) and (010) + (110), at $2\theta \cong 20.5^\circ$and 24.0° characteristic of the α crystalline form. However, the peak values of these reflections of p-MWNTs/PA6 composite are lower than that of PA6, which is attributed to the presence of MWNTs. Owing to the better compatibility between f-MWNTs with PA6, the peak positions of these reflections of f-MWNTs/PA6 remain almost unchanged as compared to PA6. In addition, amino-functionalization of MWNTs decreases the (100) reflections. These results indicate that the PA6 and MWNTs/PA6 composites have the same crystalline structure.

Crystalline morphology

The morphology of crystallization was observed by PLM and the photographs of PA6 and various MWNTs/PA6 composites are shown in Figure 11. It is found that the radius of PA6 is not uniform. The smaller crystals are only several micrometers, but the larger spherulites with a radius ∼ 25 μm also can be observed. When MWNTs are added to PA6, the radius of spherulite reduces significantly. This reduction of crystal size is more obvious for p-MWNTs/PA6 composite as shown in Figure 11(b). The dark blocks are the larger aggregations of p-MWNTs which confine the development of spherulites leading to the smaller crystals. After grafting HMD, the compatibility between f-MWNTs and PA6 is enhanced and the dispersion of f-MWNTs in PA6 is improved as supported by the smaller aggregations in Figure 11(c). Better dispersion of f-MWNTs decrease the restriction of spherulites growth, larger crystals are formed in f-MWNTs/PA6 than in p-MWNTs/PA6 composite. Interestingly, some spherulites are found [Fig. 11(c), denoted by the circles], which grows using the small aggregation of MWNTs as nucleus, thus giving a strong evidence for the heterogeneous nucleation effect of MWNTs.

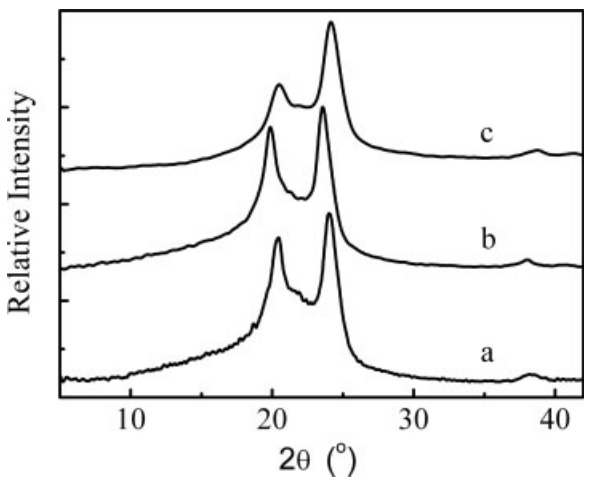

Figure 10 XRD patterns for (a) PA6 (b) p-MWNTs/PA6 and (c) f-MWNTs/PA6 composites with 1.0 wt % MWNTs after isothermal crystallization at 190 °C for 2 h.

The average dimensions of the spherulites have been determined from the H_v patterns using the following the equation

$$R_{\text{sph}} = c\lambda/(n\pi \sin Q_m) \tag{12}$$

where R_{sph} is the average spherulite radius, c a constant (c = 2.05 for spheres), λ/n the wavelength of the light in a medium of refractive index n, Q_m the angle of the incident and scattered beams corresponding to the maximum intensity. The average radius of the PA6 spherulites decreases from ∼ 8 to 3 μm in the presence of 1.0 wt % f-MWNTs. The large aggregations of p-MWNTs in PA6 are so many that the formation of complete spherulites is suppressed. No obvious image presents for p-MWNTs/PA6 composites with the H_v pattern.

CONCLUSIONS

The study of the isothermal crystallization and melting behavior of the MWNTs/PA6 composites shows that the MWNTs act as effective nucleating agents in PA6. The crystallization rates of the composites are increased, but the size of the spherulites is decreased. Functionalization of MWNTs improves the compatibility between PA6 and MWNTs resulting in a slower rate of crystallization and larger spherulites than p-MWNTs/PA6 composites. The values of the Avrami exponent are about 4.0, 1.7, and 2.3 for neat PA6, p-MWNTs/PA6, and f-MWNTs/PA6 compo-

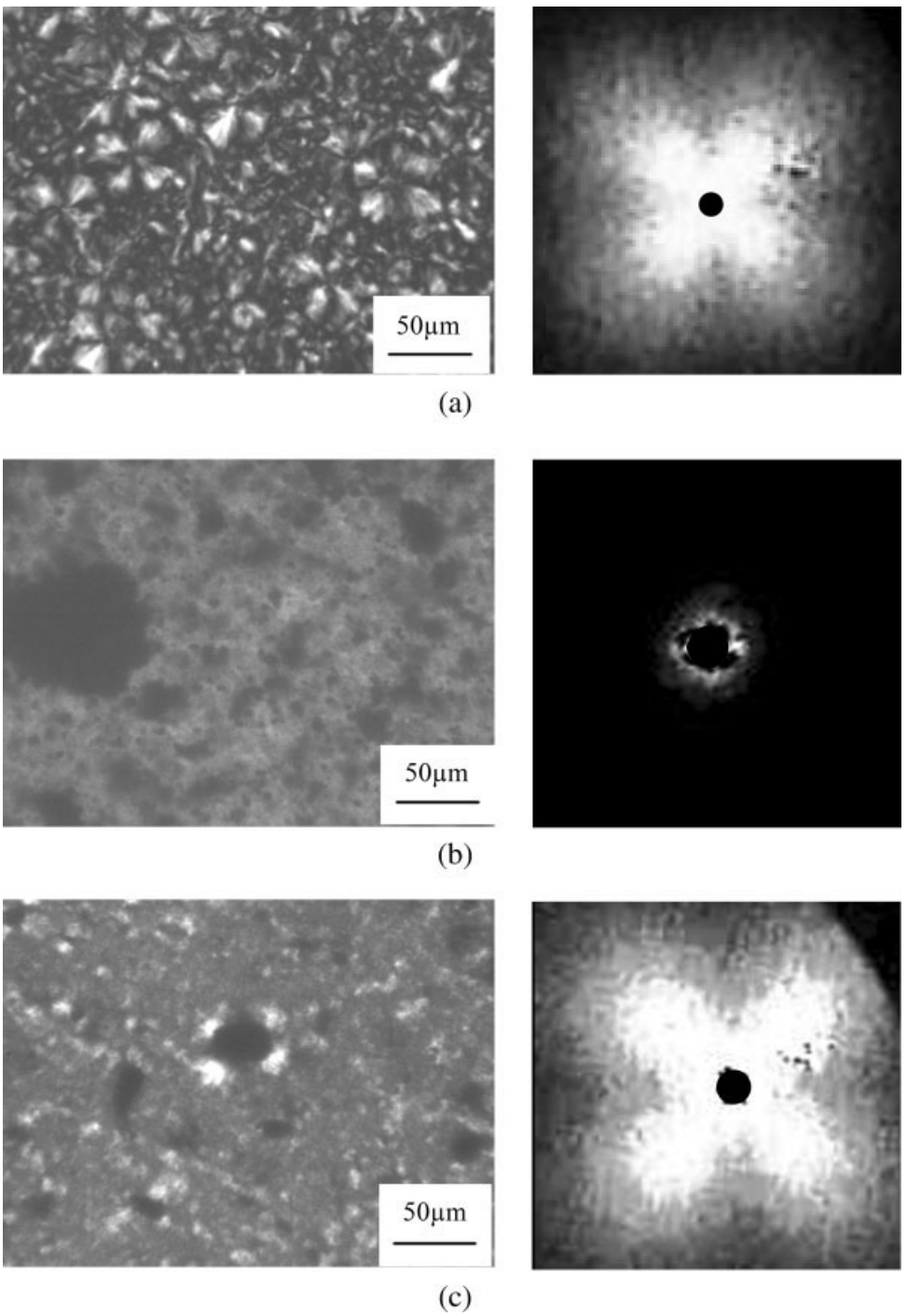

Figure 11 PLM micrographs of isothermally crystallized samples (a) PA6, (b) p-MWNTs/PA6 and (c) f-MWNTs/PA6 composites with 1.0 wt % MWNTs, the corresponding H_v patterns are also presented.

sites, respectively. It is indicated that the presence of MWNTs hinders the diffusion of PA6 chains, leading to the change of the process of crystal growth from 3D to 2D for the composites. The activation energy values of the composites are −284.71, −320.52, and −293.83 kJ/mol for neat PA6, p-MWNTs/PA6, and f-MWNTs/PA6 composites, respectively. In addition, all the samples exhibit triple melting peaks at lower temperature and double melting peaks at higher temperature. They are caused by the recrystallization of small and imperfect crystals during DSC heating. The resulting equilibrium melting temperature of PA6 is lower than its composites.

References

1. Jia, Z. J.; Wang, Z. Y.; Xu, C. L.; Liang, J.; Wei, B. C.; Wu, D. H.; Zhang, Z. M. J Tsinghua Univ (Sci Technol) 2000, 40, 14.

2. Zhang, W.; Shen, L.; Phang, I.; Liu, T. Macromolecules 2004, 37, 256.
3. Xia, H. S.; Wang, Q.; Qiu, G. H. Chem Mater 2003, 15, 3879.
4. Barber, A. H.; Cohen, S. R.; Kenig, S.; Wagner, H. D. Compos Sci Technol 2004, 64, 2283.
5. Qian, D.; Liu, W. K.; Ruoff, R. S. Compos Sci Technol 2003, 63, 1561.
6. Lau, K.-T. Chem Phys Lett 2003, 370, 399.
7. Dyke, C. A., Tour, J. M. Chem Eur J 2004, 10, 812.
8. Hamon, M. A.; Hui, H.; Bhowmik, P.; Itkis, H. M. E.; Haddon, R. C. Appl Phys A: Mater Sci Process 2002, 74, 333.
9. Steven, J. L.; Huang, A. Y.; Peng, H. Q.; Chang, I. W.; Khabashesku, V. N.; Margrave, J. L. Nano Lett 2003, 3, 331.
10. Hill, D. E.; Rao, A. M.; Allard, L. F.; Sun, Y. P. Macromolecules 2002, 35, 9466.
11. Huang, W.; Fernando, S.; Allard, L. F.; Sun, Y. Nano Lett 2003, 3, 565.
12. Gojny, F. H.; Nastalczyk, J.; Roslaniec, Z.; Schulte, K. Chem Phys Lett 2003, 370, 820.
13. Lin, Y.; Zhou, B.; Fernando, K. A. S.; Liu, P.; Allard, L. F.; Sun, Y. Macromolecules 2003, 36, 7199.
14. Mitchell, C. A.; Bahr, J. L.; Arepalli, S.; Tour, J. M.; Krishnamoorti, R. Macromolecules 2002, 35, 8825.
15. Li, J.; Fang, Z. P.; Tong, L. F.; Gu, A. J.; Liu, F. Acta Phys Chim Sin 2005, 21, 1239.
16. Li, J.; Fang, Z. P.; Tong, L. F.; Gu, A. J.; Liu, F. J Appl Polym Sci, to appear.
17. Miyasaka, K.; Ishikawa, K. J. Polym Sci 1968, A-2, 6, 1317.
18. Miyasaka, K.; Ishikawa, K. J. Polym Sci 1972, A-2, 10, 1497.
19. Murthy, N. S. Polym Commum 1991, 32, 301.
20. Brucato, V.; Crippa, G.; Picearolo, S.; Titomanlo, G. Polym Eng Sci 1991, 31, 1411.
21. Samon, J. M.; Schultz, J. M.; Wu, J.; Hsiao, B. S.; Yeh, H.; Kolb, R. J Polym Sci Part B: Polym Phys 1999, 37, 1277.
22. Matyi, R. J.; Cryst, B., Jr. J Polym Sci Polym Phys Ed 1978, 16, 1329.
23. Park, J. B.; Devries, K. L.; Statton, W. O. J.; Macromol Sci Phys B 1978, 15, 229.
24. Baldrian, J.; Pelzbauer, Z. J Polym Sci Part C: Polym Symp 1972, 38, 289.
25. Murthy, N. S.; Minor, H.; Latif, R. A. J. Mamomol Sci Phys B 1987, 28, 427.
26. Wu, T.-M.; Lien, Y.-H.; Hsu, S.-F. J Appl Polym Sci 2004, 94, 2196.
27. Zheng, J. R.; Siegel, R. W.; Toney, C. G. J Polym Sci Part B: Polym Phys 2003, 41, 1033.
28. Weng, W. G.; Chen, G. H.; Wu, D. J. Polymer 2003, 44, 8119.
29. Assouuline, E.; Lustiger, A.; Barber, A. H.; Cooper, C. A.; Klein, E.; Wachtel, E.; Wagner, H. D. J Polym Sci Part B: Polym Phys 2003, 41, 520.
30. Probst, O.; Moore, E. M.; Resasco, D. E.; Grady, B. P. Polymer 2004, 45, 4437.
31. Li, S.-N.; Li, Z.-M.; Yang, M.-B.; Hu, Z.-Q.; Xu, X.-B.; Huang, R. Mater Lett 2004, 58, 3967.
32. Liu, T. X.; Phang. I. Y.; Shen, L.; Chow, S. Y.; Zhang, W. D. Macromolecules 2004, 37, 7214.
33. Geil, P. H. Polymer Single Crystals. Wiley: New York, 1968.
34. Avrami, M. J Chem Phys 1940, 8, 212.
35. Avrami, M. J Chem Phys 1939, 7, 1103.
36. Wunderlich, B. I. Thermal Characterization of Polymeric Materials, 2nd ed.; Academic Press: New York, 1997.
37. Hoffman, J. D.; Davis, G. T.; Lauritzen, J. I. In Treatise on Solid State Chemistry: Crystalline and Noncrystalline Solid, Vol. 3; Hannay, N. B., Ed.; Plenum: New York, 1976.
38. Mucha, M.; Krolikowski, Z. J Therm Anal Cal 2003, 74, 549.
39. Lin, C. C. Polym Eng Sci 1983, 23, 113.
40. Cebe, P.; Hong, S. D. Polymer 1986, 27, 1183.
41. Wunderlich, B. I. Macromolecular Physics, Vol. 3, Crystal Melting; Academic Press: New York, 1980.
42. Liu, M. Y.; Zhao, Q. X.; Wang, Y. D.; Zhang, C. G.; Mo, Z. S.; Cao, S. K. Polymer 2003, 44, 2537.
43. Gaceva, G. B.; Janevski, A.; Grozdanov, A. J Appl Polym Sci 1997, 67, 395.
44. Murthy, N. S.; Curran, S. A.; Aharoni, S. M.; Minor, H. Macromolecules 1991, 24, 3215.
45. Khanna, Y. P. Macromolecules 1992, 25, 3298.
46. Medellín-Rodríguez, F. J.; Larios-López, L.; Zapata-Espinoza, A.; Dávalos-Montoya, O.; Phillips, P. J.; Lin, P. S. Macromolecules 2004, 37, 1799.
47. Hoffman, J. D.; Weeks, J. J. J Res Nat Bur Stand A 1962, 73, 64.